Magnetic Resonance Imaging 94 (2022) 56–63

Contents lists available at ScienceDirect

Magnetic Resonance Imaging

journal homepage: www.elsevier.com/locate/mri

MR imaging for shoulder diseases: Effect of compressed sensing and deep learning reconstruction on examination time and imaging quality compared with that of parallel imaging

Yuki Obama [a,*], Yoshiharu Ohno [a,b], Kaori Yamamoto [c], Masato Ikedo [c], Masao Yui [c], Satomu Hanamatsu [a], Takahiro Ueda [a], Hirotaka Ikeda [a], Kazuhiro Murayama [b], Hiroshi Toyama [a]

[a] Department of Radiology, Fujita Health University, School of Medicine, Japan
[b] Joint Research Laboratory of Advanced Medical Imaging, Fujita Health University, School of Medicine, Japan
[c] Canon Medical Systems Corporation, Japan

ARTICLE INFO

Keywords:
Compressed sensing
Deep learning
Parallel imaging
MRI

ABSTRACT

Purpose: To compare capabilities of compressed sensing (CS) with and without deep learning reconstruction (DLR) with those of conventional parallel imaging (PI) with and without DLR for improving examination time and image quality of shoulder MRI for patients with various shoulder diseases.
Methods and materials: Thirty consecutive patients with suspected shoulder diseases underwent MRI at a 3 T MR system using PI and CS. All MR data was reconstructed with and without DLR. For quantitative image quality evaluation, ROI measurements were used to determine signal-to-noise ratio (SNR) and contrast-to-noise ratio (CNR). For qualitative image quality assessment, two radiologists evaluated overall image quality, artifacts and diagnostic confidence level using a 5-point scoring system, and consensus of the two readers determined each final value. Tukey's HSD test was used to compare examination times to establish the capability of the two techniques for reducing examination time. All indexes for all methods were then compared by means of Tukey's HSD test or Wilcoxon's signed rank test.
Results: CS with and without DLR showed significantly shorter examination times than PI with and without DLR ($p < 0.05$). SNR and CNR of CS or PI with DLR were significantly higher than of those without DLR ($p < 0.05$). Use of DLR significantly improved overall image quality and artifact incidence of CS and PI ($p < 0.05$).
Conclusion: Examination time with CS is shorter than with PI without deterioration of image quality of shoulder MRI. Moreover, DLR is useful for both CS and PI for improvement of image quality on shoulder MRI.

1. Introduction

Magnetic resonance imaging (MRI) is the standard diagnostic modality that provides a comprehensive and accurate assessment for both osseous and soft-tissue pathologic conditions of the shoulder. Currently, MRI is considered the most comprehensive noninvasive imaging test available to evaluate shoulder abnormalities [1–13]. This modality is highly accurate for diagnosing rotator cuff disease, which is the most common cause of shoulder pain in older adults [1–6]. Specifically, MRI is effective for detecting partial-thickness and full-thickness rotator cuff tears, glenoid labral abnormalities, and other common causes of shoulder pain, such as biceps tendon tears and osteoarthritis of the glenohumeral or acromioclavicular joints [1–13]. Despite its excellent diagnostic capabilities, the high cost of MRI and limited availability of MRI scanners can constitute obstacles for its use. Therefore, a fast 5-min shoulder MRI protocol at a 1.5 T or 3 T system was introduced which uses conventional parallel imaging (PI), and a multi-reader and multi-institutional study showed that this fast 5-min shoulder MRI, with its similar inter-reader agreement and accuracy, is interchangeable with standard shoulder MRI for evaluating shoulder injuries [11].

This development was followed by a few MR vendors introducing compressed sensing (CS) as a new clinical method for reducing the

* Corresponding author at: Department of Radiology, Fujita Health University, School of Medicine, 1-98 Dengakugakubo, Kutsukake-cho, Toyoake, Aichi 470-1192, Japan.
E-mail address: y-obama@fujita-hu.ac.jp (Y. Obama).

https://doi.org/10.1016/j.mri.2022.08.004
Received 5 April 2022; Received in revised form 3 July 2022; Accepted 2 August 2022
Available online 5 August 2022

number of k-space samples by exploiting signal compressibility or compensating for sparsity in an appropriate transform domain [14–16]. This method is applicable for not only neuro, but also head and neck or pelvic MRI [15,16]. However, one of the drawbacks of CS is a relatively lower SNR than for PI. Canon Medical Systems Corporation has therefore combined CS with PI in the form of Compressed SPEEDER to provide better images than obtainable with CS alone. In addition, a few MR vendors also introduced deep learning reconstruction (DLR) to improve imaging quality not only for central nervous system, but also for body MRIs [15,17–19]. Canon Medical Systems Corporation has also developed a DLR method known as the Advanced intelligent Clear-IQ Engine (AiCE) [15,18,19]. AiCE is trained using vast amounts of high-quality image data and features a deep learning neural network that can reduce noise and boost signals to quickly deliver sharp, clear and distinct images. AiCE makes it possible to differentiate a true signal from noise through deep learning innovation to match the spatial resolution and low-noise properties of advanced scanning and reconstruction, while maintaining the true structure of the anatomy [15,16,19]. In addition, it is fully integrated with deep learning reconstruction for MRI and is built directly into the scan protocols for a seamless workflow. To date, no studies have evaluated the performance of CS (using Compressed SPEEDER) and DLR (using AiCE) for shoulder MRI in comparison to conventional PI.

We hypothesized that CS (using Compressed SPEEDER) and the DLR method can improve image quality and examination time of shoulder MRI in comparison with conventional PI. The purpose of this study was thus to compare capabilities of compressed sensing (CS) with and without deep learning reconstruction (DLR) with those of conventional parallel imaging (PI) with and without DLR for improving examination time and image quality of shoulder MRI for patients with various shoulder diseases.

2. Materials and methods

2.1. Protocol, support and funding

This retrospective study was approved by the Institutional Review Board of Fujita Health University Hospital. This study was also technically and financially supported by Canon Medical Systems Corporation. The IRB waived the need for written informed consent from all subjects in the study. Three of the authors are employees of Canon Medical Systems (K.Y., M.I. and M.Y.) but did not have control over any of the data used in this study.

2.2. Subjects

Between August 2019 and February 2020, 30 consecutive patients with suspected shoulder diseases, consisting of 20 males (mean age 57 years, range 22–83 years) and 10 females (mean age 73 years, range 58–88 years), were examined for various shoulder diseases at a 3 T MR system in our hospital. The inclusion criteria were: 1) 18 years or older, and 2) shoulder MRI performed by CS with PI and PI alone at a single examination and reconstructed with and without DLR. No patients were excluded during this study. The patient flow chart is shown in Fig. 1. Details of patient characteristics are shown in Table 1.

Table 1
MR Protocol for this study.

Protocol	Shoulder MRI with CS	Shoulder MRI with PI
Sequence	Proton density (PD)-weighted fast spin-echo (FSE)	
For fat suppression	CHESS	
TR (ms)	1800–2447	
TE (ms)	12	
Echo train length	4	
Echo spacing (ms)	12	
Flip angle (degree)	90/140	
Acceleration method	Compressed SPEEDER	SPEEDER
Reduction factor		
Phase direction	3	1.5
Slice direction	1	1
k-Space encoding	CS with PI	PI
Slice thickness (mm)	3	
Slice gap (mm)	0.6	
Slice number	19–26	
FOV (mm)	200 × 200	
Acquisition matrix	224 × 320	
Reconstruction matrix	640 × 640	
Reconstruction voxel size (mm^3)	0.5 × 0.5 × 3	
Mean acquisition time (s)	77.2 (ranged from 70 to 96)	162.5 (ranged from 144 to 201)

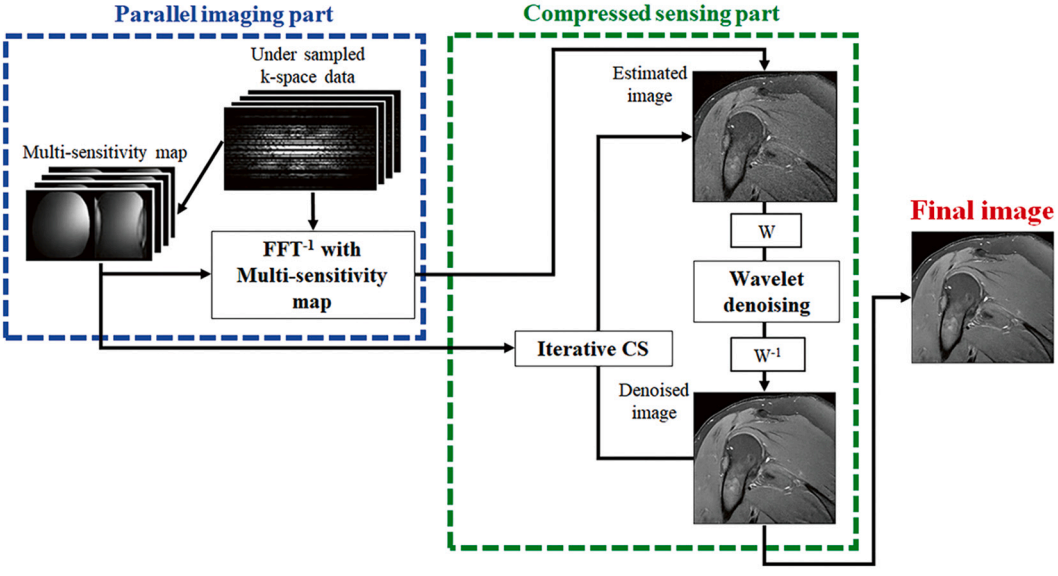

Fig. 1. Reconstruction flowchart of CS (using Compressed SPEEDER).
Schematic showing details of CS which was used in this study and consisted of a parallel imaging acquisition stage and a compressed sensing stage.

2.3. MR imaging

All MR examinations were performed at a 3 T MR system, Vantage Galan 3 T/ZGO (Canon Medical Systems Corporation, Otawara, Japan) with a 16-channel flexible SPEEDER coil. We followed the procedures described in previous literature [1–13] to perform standard shoulder MR examinations for each of the patients. For this study, we obtained fat suppressed proton density (PD)-weighted fast spin-echo (FSE) imagings with conventional PI (SPEEDER: Canon Medical Systems) and CS with PI (Compressed SPEEDER: Canon Medical Systems). Each patient underwent fat-suppressed PD-weighted FSE imaging performed with the following protocol: repetition time (TR)/echo time (TE) 1800–2447 ms/12 ms, flip angle 90/140 degrees, field of view (FOV) 200 × 200 mm, slice thickness: 3 mm, slice gap: 0.6 mm, slice number 19–26, 224 × 320 matrix (with no phase wrap), 640 × 640 reconstruction matrix. For fat suppression, the chemical shift-selective (CHESS) technique was used for each examination. CS with PI was performed with CS reduction factor 3 (i.e., k space undersampling rate [= number of echoes with CS/without CS] = 33.0% (= 148/448), and PI was performed with reduction factor 1.5 (i.e., k space undersampling rate = 71.4% (= 320/448). PD-weighted FSE data obtained with the two methods were then reconstructed with and without DLR (i.e., AiCE, Canon Medical Systems). Details of the scanning protocol are listed in Table 1.

2.4. Compressed sensing (using Compressed SPEEDER)

For CS used in this study, two-dimensional FSE imaging was performed with random undersampling in the phase encoding direction. For the first reconstruction stage, one of the PIs is used for CS and estimated multiple sensitivity maps using fully sampled echoes around the central k-space are obtained, followed by image-domain parallel reconstruction applied to all the acquired echoes [15,16,20]. This reconstruction process is shown in the parallel imaging stage of Fig. 1. Some artifacts and excess noise due to undersampling in k-space are still seen on the images generated from the first reconstruction stage, and are eliminated in the second stage, shown as the "Compressed sensing stage" in Fig. 1, where the estimated image is resolved by using a wavelet transform and an iterative CS optimization with least absolute shrinkage and selection operator (LASSO) regression [15,16,21]. Multiple sensitivity maps are also used in the second stage to maintain consistency of all the acquired data during the iterative process. Details of our CS have been described in previous reports [15,16].

2.5. Deep learning reconstruction (using advanced intelligent clear-IQ engine [AiCE])

The DLR used in our study is a variety of the convolutional neural networks (CNNs) and dedicated to image denoising with preserved anatomical information. The denoising process flow of the DLR architecture is shown in Fig. 2 and is integrated in the whole reconstruction pipeline after raw complex data acquisition until final image generation. The neural network of DLR has three types of layers. First, the input image is processed in the feature extraction layer with a discrete-cosine-transform (DCT) convolution and with soft shrinkage activation only for high-frequency DCT components. The DCT convolution block internally generates 49 components of each input image with a fixed 7 × 7 DCT basis. Soft shrinkage activation is applied to the 48 high-frequency DCT components of the image, except for the zero-frequency component. Second, the 48 DCT components are further processed by using multiple feature conversion layers. Each feature conversion layer has a convolution block with a kernel size of 3 × 3 and a soft shrinkage block. Finally, in the image generation layer, the denoised image is generated by deconvolution of the 48 noise-reduced components and the original zero-frequency component with a 7 × 7 inverse DCT kernel. The soft shrinkage of the DLR is noise adaptive, which means that a variable threshold of an inactive section is determined by the amount of noise [15,18,22]. Hence, the DLR network has two kinds of learned parameters: one consists of the 3 × 3 convolution kernels in the feature conversion layers and the other of the coefficients of the soft shrinkage activation function in the feature extraction layer and the feature conversion layers. These parameters are determined by minimizing the loss function through a training process. In this study, the same training network of the DLR was used as described elsewhere [15,18], where details of our DLR can also be found.

The DLR network was trained by a pair of a high-SNR ground-truth image and a noisy input image. The high-SNR ground-truth images were

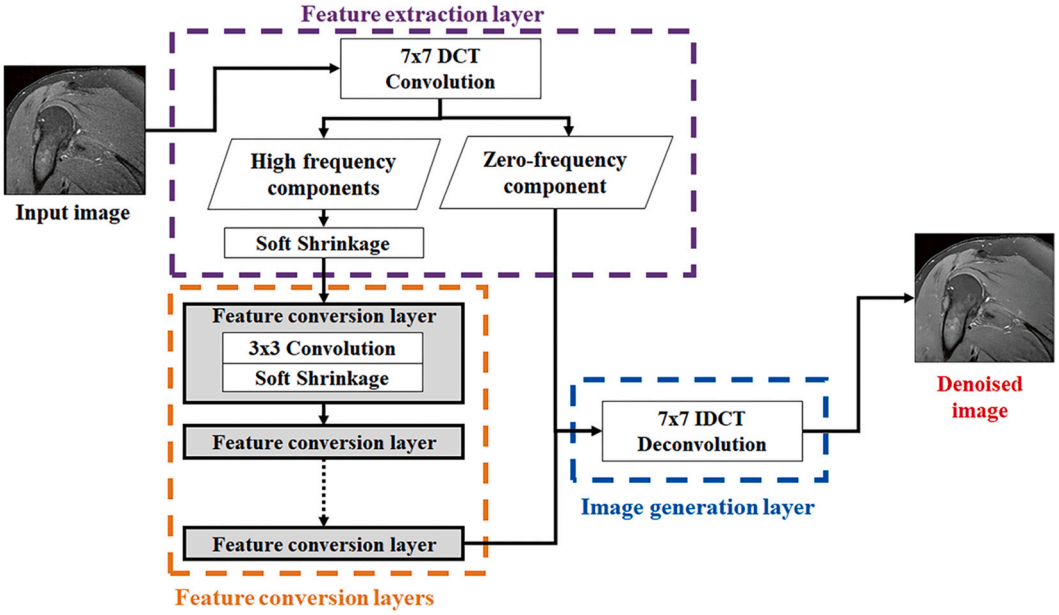

Fig. 2. Flow chart for deep learning reconstruction method (using AiCE).
In the first feature extraction layer, the input image is convolved by a 7 × 7 DCT kernel. After the first soft shrinkage, 48 high frequency components repeatedly undergo 3 × 3 convolution and soft shrinkage in the feature conversion layers. Finally, the denoised output image is generated by IDCT deconvolution of both the bypassed zero-frequency component and the output data from the feature conversion layers.

generated by ten-times averaging of images acquired with various contrast of T1W, T2W, FLAIR for brain, and T2W, T2*W, PDW, fat saturated PDW for knee. The noisy input images were generated from the ground-truth images by adding Gaussian noise with various noise level. Data augmentation was also applied by flipping the training image pairs. Training image pairs were divided to nine image patches, and finally 32,400 training two-dimensional image pairs were obtained [18].

2.6. Image analysis

All quantitative and qualitative assessments of image quality were performed on a commercially available picture archiving and communication system (PACS) (RapideyeCore; Canon Medical Systems).

For quantitative image quality assessment, regions of interests (ROIs) with the same diameter were placed over the humeral head and supraspinatus muscle by a board-certified muscle skeletal radiologist (Y.O.) with 10 years' experience (Fig. 3). For quantitative image quality assessment, signal-to-noise ratio (SNR) and percentage of coefficient of variation (%CV) of the humeral head and contrast-to-noise ratio (CNR) between the humeral head and supraspinatus muscle were calculated by using the following formulas derived from previous reports [15,16,23].

$$\mathrm{SNR} = \mathrm{SI}_{\text{Humeral head}} / \mathrm{SD}_{\text{Supraspinatus muscle}} \quad (1)$$

$$\%\mathrm{CV}\ (\%) = \mathrm{SD}_{\text{Supraspinatus muscle}} / \mathrm{SI}_{\text{Humeral head}} \times 100 \quad (2)$$

where $\mathrm{SI}_{\text{Humeral head}}$ is the averaged signal intensity of the humeral head within the ROI, and $\mathrm{SD}_{\text{Supraspinatus muscle}}$ is the average standard deviation of the supraspinatus muscle within the ROI.

And for CNR:

$$\mathrm{CNR} = \mathrm{SNR}_{\text{Humeral head}} - \mathrm{SNR}_{\text{Supraspinatus muscle}} \quad (3)$$

where $\mathrm{SNR}_{\text{Humeral head}}$ is the SNR of the humeral head within the ROI placed on each humeral head and supraspinatus muscle, and $\mathrm{SNR}_{\text{Supraspinatus muscle}}$ is the SNR of the supraspinatus muscle.

For qualitative assessment of image quality, the same board-certified musculoskeletal radiologist and a board-certified chest radiologist (Yo. Oh.) with 27 years' experience independently and visually evaluated overall image quality, artifact incidence and diagnostic performance by using a 5-point scoring system. To assess qualitative indexes, all images obtained with PI and CS and reconstructed with and without DLR were randomized without any information for acquisition and reconstruction methods. For this study, overall image quality was rated as: 1, poor; 2, fair; 3, moderate; 4, good; and 5, excellent. Artifacts were scored as: 1, no visualization of artifacts; 2, visualization of few artifacts; 3, visualization of some artifacts; 4, visualization of several artifacts; and 5, visualization of significant numbers of artifact. Diagnostic confidence level was rated as: 1, ≤20% confidence (i.e. very unsure); 2, 21–40% confidence; 3, 41–60% confidence; 4, 61–80% confidence; and 5, 81% ≤ confidence (i.e. highly confident). All final visual scores for every patient were determined by consensus of the two readers.

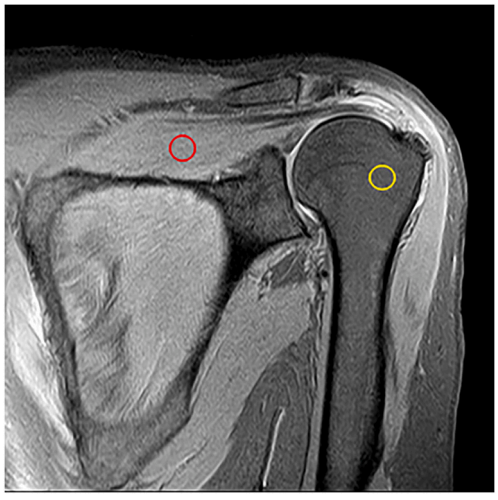

Fig. 3. 44-year-old male patient with rotator cuff injury.
On fat-suppressed PD-weighted image obtained by PI without DLR, regions of interests (ROIs) with the same diameter were placed over the humeral head (yellow circle) and supraspinatus muscle (red circle). (For interpretation of the references to colour in this figure legend, the reader is referred to the web version of this article.)

2.7. Statistical analysis

To determine differences in mean examination time for all methods, the times needed for examination using the various methods were compared by means of Tukey's honestly significant difference (HSD) test.

For a comparison of quantitative image quality indexes for all methods, SNR, %CV and CNR of the methods were compared using Tukey's HSD test.

To determine inter-observer agreement on assessments of qualitatively assessed image quality indexes, agreements on overall image quality, artifacts and diagnostic confidence level were evaluated by kappa statistics followed by the χ^2 test. Agreements were assessed as: poor for $\kappa < 0.21$, fair for $\kappa = 0.21$–0.40, moderate for $\kappa = 0.41$–0.60, substantial for $\kappa = 0.61$–0.80, and excellent for $\kappa = 0.81$–1.00 [24].

For a comparison of all qualitative image quality indexes, median scores for overall image quality, artifact and diagnostic confidence level were compared among the various methods by means of Wilcoxon signed-rank test.

A p value <0.05 was considered significant for all statistical analyses.

3. Results

All MR data were obtained with CS and PI and reconstructed with and without DLR. No adverse effects were observed in this study. Details of patient characteristics are shown in Table 2. Representative cases are shown in (Figs. 4 and 5).

Mean examination times for shoulder MRI obtained with CS and PI and reconstructed with and without DLR are shown in Table 3. Mean examination time for CS with DLR (82.8 ± 5.2 s) was significantly shorter than for PI with and without DLR (with DLR: 166.2 ± 11.7 s, $p < 0.0001$; without DLR: 162.5 ± 11.1 s, $p < 0.0001$), while mean examination time for CS without DLR (77.2 ± 4.7 s) was significantly shorter than for PI with and without DLR (with DLR: $p < 0.0001$, without DLR: $p < 0.0001$). Moreover, mean examination time for PI was significantly shorter than that for CS with and without DLR ($p < 0.0001$).

A comparison of all quantitative image quality indexes for all methods is shown in Table 4. SNR (21.0 ± 9.4), %CV (5.9 ± 3.0) and CNR (12.8 ± 6.7) for CS with DLR were significantly better than those for CS without DLR (SNR: 10.8 ± 4.7, $p < 0.0001$; %CV: 10.7 ± 4.1, $p < 0.0001$; CNR: 6.7 ± 4.0, $p < 0.0001$) and PI without DLR (SNR: 12.1 ±

Table 2
Patient Characteristics.

Gender	Male	20
	Female	10
Age (years)	Mean ± SD (range)	64 ± 15 (22–88)
Diseases (Cases)	Rotator cuff injury	20
	Periarthritis	3
	Calcific tendinitis	3
	Greater tuberosity fracture	2
	Biceps tendon injury	1
	Shoulder dislocation	1

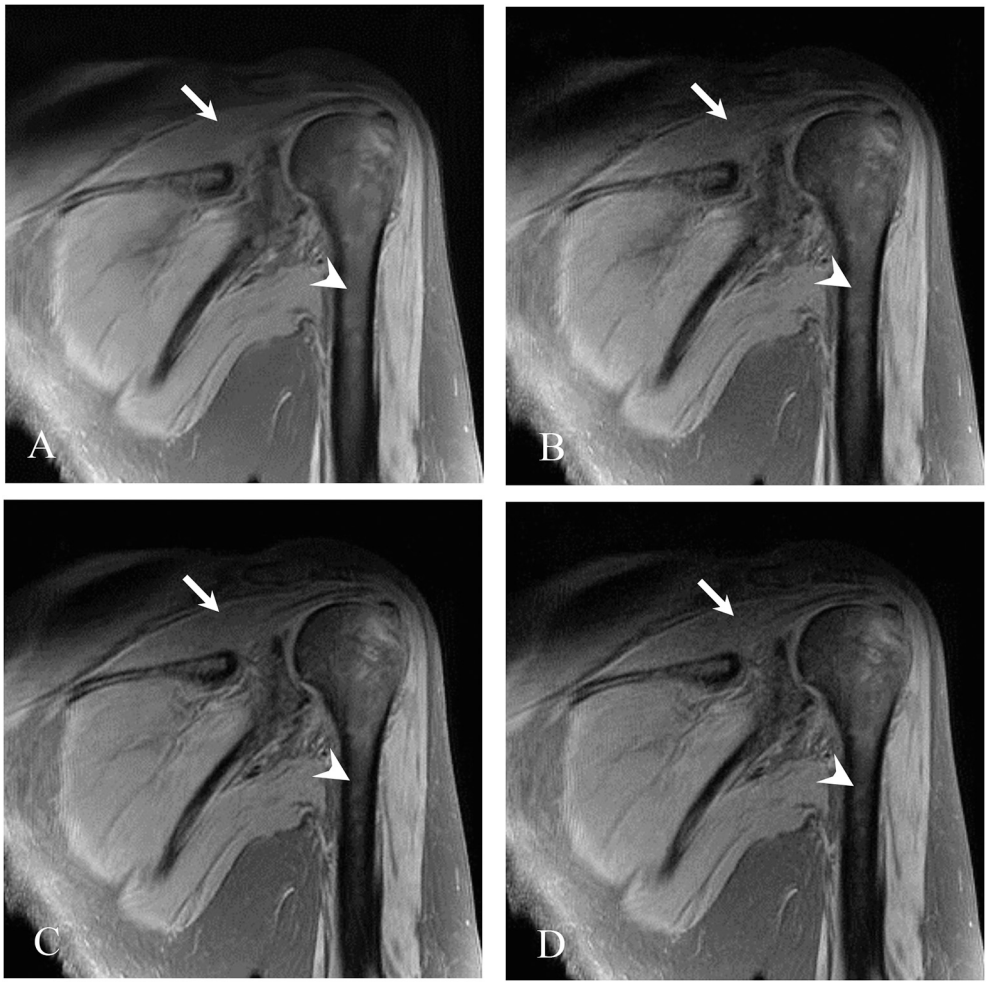

Fig. 4. 67-year-old female patient with greater tuberosity fracture.
A) CS with DLR; B) CS without DLR; C) PI with DLR; and D) PI without DLR. Each of the fat-suppressed PD-weighted images shows high signal intensity at the greater tubercle of the humerus and was diagnosed as a greater tuberosity fracture. DLR reduced image noise on fat-suppressed PD-weighted images obtained by CS and PI, and markedly improved visualization of bone marrow (arrowhead) and muscle (arrow). SNRs of all methods were assessed as: CS with DLR, 27.6; CS without DLR, 11.7; PI with DLR, 14.7; and PI without DLR, 8.7. Overall image quality and artifacts for each method were determined as: CS with DLR, 5 and 1; CS without DLR, 4 and 2; PI with DLR, 4 and 2; and PI without DLR, 3 and 3. Examination times were: CS with DLR, 83 s; CS without DLR, 78 s; PI with DLR, 169 s; and PI without DLR, 164 s.

5.0, $p < 0.0001$; %CV: 9.7 ± 4.5, $p < 0.0001$; CNR: 7.4 ± 4.4, $p < 0.0001$). SNR (19.9 ± 9.0), %CV (6.0 ± 2.6) and CNR (12.0 ± 5.9) PI with DLR were significantly worse than those for CS without DLR (SNR: $p < 0.0001$, %CV: $p < 0.0001$, CNR: $p < 0.0001$), while SNR, %CV and CNR for PI with DLR were significantly better than those for PI without DLR (SNR: $p = 0.0004$, %CV: $p = 0.0009$, CNR: $p = 0.007$).

Interobserver agreements for each qualitative index are shown in Table 5. For overall image quality evaluation, interobserver agreements for CS with DLR ($\kappa = 0.65$, $p < 0.0001$) and without DLR ($\kappa = 0.74$, $p < 0.0001$) and PI with DLR ($\kappa = 0.79$, $p < 0.0001$) were significant and substantial, and those for PI without DLR ($\kappa = 0.83$, $p < 0.0001$) were significant and almost perfect. As for artifact assessments, interobserver agreements for CS with DLR ($\kappa = 0.65$, $p < 0.0001$) and without DLR ($\kappa = 0.74$, $p < 0.0001$) and PI with DLR ($\kappa = 0.79$, $p < 0.0001$) were significant and substantial, while agreement for PI without DLR ($\kappa = 0.83$, $p < 0.0001$) was significant and almost perfect. Evaluations of diagnostic confidence level showed that interobserver agreements for CS with DLR ($\kappa = 0.65$, $p < 0.0001$) and PI without DLR ($\kappa = 0.63$, $p < 0.0001$) were significant and substantial, and those for CS without DLR ($\kappa = 0.50$, $p < 0.0001$) and PI without DLR ($\kappa = 0.59$, $p < 0.0001$) significant and moderate.

Table 6 shows a comparison of qualitative indexes. Overall image quality for CS with DLR (median: 5) was significantly better than that for CS without DLR (median: 4, $p < 0.0001$) and PI without DLR (median: 4, $p < 0.0001$), and significantly better for PI with DLR (median: 5) than that for CS without DLR ($p = 0.0003$) and PI without DLR ($p = 0.0008$). As for artifacts, CS with DLR (median: 5) showed significantly fewer artifacts than did CS without DLR (median: 4, $p < 0.0001$) and PI without DLR (median: 4, $p < 0.0001$). PI with DLR (median: 5) showed significantly fewer artifacts than did CS without DLR ($p = 0.0003$) and PI without DLR ($p = 0.0008$). Finally, a comparison of diagnostic confidence levels showed no significant differences among the methods ($p > 0.05$).

4. Discussion

Our results demonstrate that the capability of CS (using Compressed SPEEDER) and DLR (using AiCE) as compared with that of PI (using SPEEDER) was greater for reducing examination time and improving quantitative and qualitative image quality for undersampled k-space data for shoulder MRI without deterioration of diagnostic confidence level. To the best of our knowledge, no studies have been reported that evaluated the utility of the aforementioned techniques for shoulder MRI in routine clinical practice.

A comparison of mean examination times for CS and PI reconstructed with and without DLR demonstrated that mean examination times for CS with and without DLR were significantly shorter than those for PI reconstructed with and without DLR. PI (using SPEEDER) as well as similar parallel imaging methods from other vendors is well known as a method which uses the spatial sensitivity of each receiver in a multi-coil array, reconstructs the MR image from undersampled k-space data, and reduces MR acquisition time [14–16,25–27]. On the other hand, CS (using Compressed SPEEDER) exploits sparsity in MR images to recover MR images from undersampled k-space data, and the wavelet transformation domain can reduce image noise and maintain image quality by applying a given threshold [14–16,25–27]. Our results show that the

Fig. 5. 44-year-old male patient with rotator cuff injury.
A) CS with DLR; B) CS without DLR; C) PI with DLR; and D) PI without DLR. Each of the fat-suppressed PD-weighted images shows high signal intensity of the rotator cuff and was diagnosed as a rotator cuff injury (arrow). Image quality for CS without DLR was slightly lower than for the other methods. SNRs of all methods were assessed as: CS with DLR, 16.7; CS without DLR, 9.5; PI with DLR, 13.8; PI without DLR, 9.9. Overall image quality and artifacts for each method were determined as: CS with DLR, 5 and 1; CS without DLR, 4 and 2; PI with DLR, 5 and 1; and PI without DLR, 5 and 1. Examination times were: CS with DLR, 84 s; CS without DLR, 79 s; PI with DLR, 170 s; and PI without DLR, 165 s.

Table 3
Mean examination times for shoulder MRI obtained with CS and PI and reconstructed with and without DLR.

Method	Mean examination time (*sec*) (mean ± SD)
CS with DLR	82.8 ± 5.2
CS without DLR	77.0 ± 4.7
PI with DLR	166.2 ± 11.7*,***
PI without DLR	162.5 ± 11.1*,***

CS: Compressed sensing, DLR: Deep learning reconstruction, PI: Parallel imaging.
* Significantly different from CS with DLR ($p < 0.05$).
** Significantly different from CS without DLR ($p < 0.05$).

Table 4
Quantitative image quality indexes for all methods.

Method	SNR (mean ± SD)	%CV (mean ± SD)	CNR (mean ± SD)
CS with DLR	21.0 ± 9.4	5.9 ± 3.0	12.8 ± 6.7
CS without DLR	10.8 ± 4.7*	10.7 ± 4.1*	6.7 ± 4.0*
PI with DLR	19.9 ± 9.0**	6.0 ± 2.6**	12.0 ± 5.9**
PI without DLR	12.1 ± 5.0*,***	9.7 ± 4.5*,***	7.4 ± 4.4*,***

SNR: Signal-to-noise ratio, %CV: Percentage of coefficient of variation, CNR: Contrast-to-noise ratio, CS: Compressed sensing, DLR: Deep learning reconstruction, PI: Parallel imaging.
* Significantly different from CS with DLR ($p < 0.05$).
** Significantly different from CS without DLR ($p < 0.05$).
*** Significantly different from PI with DLR ($p < 0.05$).

capability of CS to reduce examination time is superior to that of PI, whether DLR is applied or not. In addition, DLR could be used without any increase in examination time for MRI obtained with each of the methods. These findings suggest that it is advisable to use CS combined with DLR for MR examinations in routine clinical practice.

The comparison of quantitative image quality evaluations showed that CS or PI reconstructed with DLR yielded significantly higher SNR and CNR and lower %CV than CS or PI reconstructed without DLR. In addition, DLR can improve image quality as well as contrast of shoulder MRI, while CS and PI had no significant effect on image quality or contrast in routine clinical practice. Therefore, the aforementioned threshold for the wavelet transformation in the case of CS may be considered significatively useful for reduction of examination time and should be used together with DLR in routine clinical practice. These conclusions are mostly compatible with those mentioned in previous literature [15,16,18].

For qualitative image quality assessments, we evaluated interobserver agreement for each index and determined that the qualitative evaluations in our study were moderate, substantial or almost perfect and can thus be considered reproducible becauseκranged from 0.50 to 0.83. Moreover, overall image quality and artifact incidence of CS or PI with DLR were significantly superior to those of CS or PI without DLR, although diagnostic confidence level showed no significant differences among any of the methods. These results suggest that image quality and artifact incidence were improved by the use of DLR, and that DLR can

Table 5
Interobserver agreement for qualitative indexes.

Qualitative index	Method	Reader	Visual score					κ	p value
			1	2	3	4	5		
Overall image quality	CS with DLR	1	0	0	1	0	29	0.65	<0.001
		2	0	0	1	1	28		
	CS without DLR	1	0	0	4	19	7	0.74	<0.001
		2	0	0	3	19	8		
	PI with DLR	1	0	1	1	3	25	0.79	<0.001
		2	0	2	0	4	24		
	PI without DLR	1	1	1	3	16	9	0.83	<0.001
		2	1	1	3	15	10		
Artifacts	CS with DLR	1	29	0	1	0	0	0.65	<0.001
		2	28	1	1	0	0		
	CS without DLR	1	7	19	4	0	0	0.74	<0.001
		2	8	19	3	0	0		
	PI with DLR	1	25	3	1	1	0	0.79	<0.001
		2	24	4	0	2	0		
	PI without DLR	1	9	16	3	1	1	0.83	<0.001
		2	10	15	3	1	1		
Diagnostic confidence level	CS with DLR	1	0	0	0	2	28	0.65	<0.001
		2	0	0	0	1	29		
	CS without DLR	1	0	0	2	4	24	0.5	<0.001
		2	0	0	1	2	27		
	PI with DLR	1	0	1	0	4	25	0.59	<0.001
		2	0	1	1	1	27		
	PI without DLR	1	1	0	2	2	25	0.63	<0.001
		2	1	0	1	2	26		

CS: Compressed sensing, DLR: Deep learning reconstruction, PI: Parallel imaging.

Table 6
Comparison of all qualitative indexes for all methods.

Method	Overall image quality	Artifacts	Diagnostic confidence level
	Median (IQR)	Median (IQR)	Median (IQR)
CS with DLR	5 [5]	1 [1]	5 [5]
CS without DLR	4* [4,5]	2* [1,2]	5 [5]
PI with DLR	5** [5]	1** [1]	5 [5]
PI without DLR	4***** [4,5]	2***** [1,2]	5 [5]

IQR: Inter Quartile Range.
CS: Compressed sensing, DLR: Deep learning reconstruction, PI: Parallel imaging.
* Significantly different from CS with DLR ($p < 0.05$).
** Significantly different from CS without DLR ($p < 0.05$).
*** Significantly different from PI with DLR ($p < 0.05$).

play a more effective role when used with MR images obtained with not only PI, but also CS for shoulder MRI in routine clinical practice. Furthermore, compared with PI, CS can reduce image acquisition time without any deterioration of image quality or diagnostic confidence level. These findings are consistent with our quantitatively assessed image quality evaluations and previously reported findings [14–16,23,26,27]. This indicates that CS (using Compressed SPEEDER) is useful for faster image acquisition without any worsening of diagnostic confidence level. Moreover, DLR can reduce image noise without any deterioration of image contrast and should be used for not only PI, but also CS in routine clinical practice. Finally, CS should be used for MRI rather than PI and also used with DLR for enhancement of MR examination in routine clinical practice.

There are a few limitations to this study. First, we tested the utility of CS and DLR for only PD-weighted imaging and did not assess other sequences in this study. Moreover, we compared MR examination time and quantitative and qualitative image quality of CS and PI and assessed the influence of DLR on MR images obtained with the two methods in this study. However, a few investigators have suggested that the deep learning method might be useful for the reconstruction of CS itself [14,15,18,28,29]. Therefore, further investigation of the use of these techniques in routine clinical practice. In addition, same CS and DLR had been tested and demonstrated their utility on women's pelvic MRI or head and neck MRI, and little technical improvement or innovation could not be added in this study, although this paper has firstly applied both technique in musculoskeletal MR field. Second, the number of subjects included in this study was limited and their underlying pathological and clinical conditions varied. Moreover, we tested CS as well as DLR to PD-weighted imaging because the latter is one of the fundamental sequences that have been suggested in the past [1–13]. Moreover, CS or DLR had been tested for T1- and T2-weighted imaging in previous studies [15,16,18]. However, we did not compare diagnostic performance of MRI using CS with and without DLR with that using PI with and without DLR, although diagnostic confidence level for shoulder MRI was assessed in this study. Therefore, this study could not compare the actual diagnostic potential of CS and PI with and without DLR. Third, we tested CS and DLR with a 3 T MR system but not with a 1.5 T MR system or other field strengths. However, these techniques are probably applicable to other field strengths, and not only to static, but also other types of MRI. In addition, we applied CS factor as 3, which was two times higher than PI factor, in this study and could not test CS factor >3. MR images obtained by CS with DLR may be increased CS factor more, when compared with that without DLR. We therefore plan to determine in the near future the real significance of CS as well as DLR for shoulder MRI in comparison with procedures currently used in routine clinical practice.

In conclusion, examination time with CS is shorter than with PI without deterioration of image quality of shoulder MRI. Moreover, DLR is useful for both CS and PI for improvement of image quality on shoulder MRI.

Funding

This work is "Original Research", and was financially or technically supported by Canon Medical Systems Corporation.

References

[1] Zlatkin MB, Iannotti JP, Roberts MC, et al. Rotator cuff tears: diagnostic performance of MR imaging. Radiology. 1989;172(1):223–9. https://doi.org/10.1148/radiology.172.1.2740508.

[2] Iannotti JP, Zlatkin MB, Esterhai JL, Kressel HY, Dalinka MK, Spindler KP. Magnetic resonance imaging of the shoulder. Sensitivity, specificity, and predictive value. J Bone Joint Surg Am 1991;73(1):17–29. Retrieved from, https://journals.lww.com/jbjsjournal.

[3] Yamamoto A, Takagishi K, Osawa T, et al. Prevalence and risk factors of a rotator cuff tear in the general population. J Shoulder Elb Surg 2010;19(1):116–20. https://doi.org/10.1016/j.jse.2009.04.006.

[4] Gyftopoulos S, Bencardino JT, Immerman I, Zuckerman JD. The rotator cable: magnetic resonance evaluation and clinical correlation. Magn Reson Imaging Clin N Am 2012;20(2):173–85. ix, https://doi.org/10.1016/j.mric.2012.01.007.

[5] Pappou IP, Schmidt CC, Jarrett CD, Steen BM, Frankle MA. AAOS appropriate use criteria: optimizing the management of full-thickness rotator cuff tears. J Am Acad Orthop Surg 2013;21(12):772–5. https://doi.org/10.5435/jaaos-21-12-772.

[6] Gyftopoulos S, Bencardino J, Nevsky G, et al. Rotator cable: MRI study of its appearance in the intact rotator cuff with anatomic and histologic correlation. AJR Am J Roentgenol 2013;200(5):1101–5. https://doi.org/10.2214/ajr.12.9312.

[7] Zanetti M, Weishaupt D, Gerber C, Hodler J. Tendinopathy and rupture of the tendon of the long head of the biceps brachii muscle: evaluation with MR arthrography. AJR Am J Roentgenol 1998;170(6):1557–61. https://doi.org/10.2214/ajr.170.6.9609174.

[8] Spencer Jr EE, Dunn WR, Wright RW, et al. Shoulder multicenter orthopaedic outcomes network. Interobserver agreement in the classification of rotator cuff tears using magnetic resonance imaging. Am J Sports Med 2008;36(1):99–103. https://doi.org/10.1177/0363546507307504.

[9] Smith TO, Drew BT, Toms AP. A meta-analysis of the diagnostic test accuracy of MRA and MRI for the detection of glenoid labral injury. Arch Orthop Trauma Surg 2012;132(7):905–19. https://doi.org/10.1007/s00402-012-1493-8.

[10] Lenza M, Buchbinder R, Takwoingi Y, Johnston RV, Hanchard NC, Faloppa F. Magnetic resonance imaging, magnetic resonance arthrography and ultrasonography for assessing rotator cuff tears in people with shoulder pain for whom surgery is being considered. Cochrane Database Syst Rev 2013 Sep 24;2013(9):CD009020. https://doi.org/10.1002/14651858.cd009020.pub2.

[11] Subhas N, Benedick A, Obuchowski NA, et al. Comparison of a fast 5-minute shoulder MRI protocol with a standard shoulder MRI protocol: a multiinstitutional multireader study. AJR Am J Roentgenol 2017;208(4):W146–54. https://doi.org/10.2214/ajr.16.17041.

[12] Expert Panel on Musculoskeletal Imaging, Small KM, Adler RS, Shah SH, et al. ACR appropriateness criteria shoulder pain-atraumatic. J Am Coll Radiol 2018;15(11S):S388–402. https://doi.org/10.1016/j.jacr.2018.09.032.

[13] Alaia EF, Subhas N. Shoulder MR imaging and MR arthrography techniques: new advances. Magn Reson Imaging Clin N Am 2020;28(2):153–63. https://doi.org/10.1016/j.mric.2019.12.001.

[14] Feng L, Benkert T, Block KT, Sodickson DK, Otazo R, Chandarana H. Compressed sensing for body MRI. J Magn Reson Imaging 2017;45(4):966–87. https://doi.org/10.1002/jmri.25547.

[15] Ueda T, Ohno Y, Yamamoto K, et al. Compressed sensing and deep learning reconstruction for women's pelvic MRI denoising: utility for improving image quality and examination time in routine clinical practice. Eur J Radiol 2021;134:109430. https://doi.org/10.1016/j.ejrad.2020.109430.

[16] Ikeda H, Ohno Y, Murayama K, et al. Compressed sensing and parallel imaging accelerated T2 FSE sequence for head and neck MR imaging: comparison of its utility in routine clinical practice. Eur J Radiol 2021;135:109501. https://doi.org/10.1016/j.ejrad.2020.109501.

[17] Qiu D, Zhang S, Liu Y, Zhu J, Zheng L. Super-resolution reconstruction of knee magnetic resonance imaging based on deep learning. Comput Methods Prog Biomed 2020;187:105059. https://doi.org/10.1016/j.cmpb.2019.105059.

[18] Kidoh M, Shinoda K, Kitajima M, et al. Deep learning based noise reduction for brain MR imaging: tests on phantoms and healthy volunteers. Magn Reson Med Sci 2020;19(3):195–206. https://doi.org/10.2463/mrms.mp.2019-0018.

[19] Yokota Y, Takeda C, Kidoh M, et al. Effects of deep learning reconstruction technique in high-resolution non-contrast magnetic resonance coronary angiography at a 3-tesla machine. Can Assoc Radiol J 2021;72(1):120–7. https://doi.org/10.1177/0846537119900469.

[20] Uecker M, Lai P, Murphy MJ, et al. ESPIRiT–an eigenvalue approach to autocalibrating parallel MRI: where SENSE meets GRAPPA. Magn Reson Med 2014;71(3):990–1001. https://doi.org/10.1002/mrm.24751.

[21] Lustig M, Donoho D, Pauly JM. Sparse MRI: the application of compressed sensing for rapid MR imaging. Magn Reson Med 2007;58(6):1182–95. https://doi.org/10.1002/mrm.21391.

[22] Isogawa K, Ida T, Shiodera T, et al. Deep shrinkage convolutional neural network for adaptive noise reduction. IEEE Signal Process Lett 2018;25:224–8. Retrieved from, https://ieeexplore.ieee.org/.

[23] Toledano-Massiah S, Sayadi A, de Boer R, et al. Accuracy of the compressed sensing accelerated 3D-FLAIR sequence for the detection of MS plaques at 3T. AJNR Am J Neuroradiol 2018;39(3):454–8. https://doi.org/10.3174/ajnr.a5517.

[24] Svanholm H, Starklint H, Gundersen HJ, Fabricius J, Barlebo H, Olsen S. Reproducibility of histomorphologic diagnoses with special reference to the kappa statistic. APMIS. 1989;97(8):689–98. https://doi.org/10.1111/j.1699-0463.1989.tb00464.x.

[25] Pruessmann KP, Weiger M, Scheidegger MB, Boesiger P. SENSE: sensitivity encoding for fast MRI. Magn Reson Med 1999;42(5):952–62. Retrieved from, https://onlinelibrary.wiley.com/journal/15222594.

[26] Sartoretti T, Reischauer C, Sartoretti E, Binkert C, Najafi A, Sartoretti-Schefer S. Common artefacts encountered on images acquired with combined compressed sensing and SENSE. Insights Imaging 2018;9(6):1107–15. https://doi.org/10.1007/s13244-018-0668-4.

[27] Jaspan ON, Fleysher R, Lipton ML. Compressed sensing MRI: a review of the clinical literature. Br J Radiol 2015;88(1056):20150487. https://doi.org/10.1259/bjr.20150487.

[28] Yang G, Yu S, Dong H, Slabaugh G, et al. DAGAN: deep De-aliasing generative adversarial networks for fast compressed sensing MRI reconstruction. IEEE Trans Med Imaging 2018;37(6):1310–21. https://doi.org/10.1109/tmi.2017.2785879.

[29] Sun L, Fan Z, Fu X, Huang Y, Ding X, Paisley J. A deep information sharing network for multi-contrast compressed sensing MRI reconstruction. IEEE Trans Image Process 2019;28(12):6141–53. https://doi.org/10.1109/tip.2019.2925288.